# Conical and glancing Jahn-Teller intersections in the cyclic trinitrogen cation

Vadim A. Mozhayskiy
*Department of Chemistry, University of Southern California, Los Angeles, California 90089-0482*

Dmitri Babikov
*Chemistry Department, Marquette University, Milwaukee, Wisconsin 53201-1881*

Anna I. Krylov[a)]
*Department of Chemistry, University of Southern California, Los Angeles, California 90089-0482*

(Received 22 March 2006; accepted 19 April 2006; published online 12 June 2006)

The ground and electronically excited states of cyclic $N_3^+$ are characterized at the equilibrium $D_{3h}$ geometry and along the Jahn-Teller distortions. Lowest excited states are derived from single excitations from the doubly degenerate highest occupied molecular orbitals (HOMOs) to the doubly degenerate lowest unoccupied molecular orbitals (LUMOs), which give rise to two exactly and two nearly degenerate states. The interaction of two degenerate states with two other states eliminates linear terms and results in a glancing rather than conical Jahn-Teller intersection. HOMO-2 $\rightarrow$LUMOs excitations give rise to two regular Jahn-Teller states. Optimized structures, vertical and adiabatic excitation energies, frequencies, and ionization potential (IP) are presented. IP is estimated to be 10.595 eV, in agreement with recent experiments. © *2006 American Institute of Physics*. [DOI: 10.1063/1.2204602]

## I. INTRODUCTION

Interest in homonuclear triatomic molecules has a long history. This is the smallest nonlinear system that can have a non-Abelian point group symmetry containing irreducible representations of the order higher than one, which results in symmetry required degeneracies between some electronic states at high symmetry geometries ($D_{3h}$ or equilateral triangle) and the intersections between the corresponding potential energy surfaces (PESs).

According to the Jahn-Teller (JT) theorem,[1–3] high symmetry intersection points in nonlinear systems are not stationary points on PESs, that is, degenerate states follow first order JT distortions to a lower symmetry, which lifts the degeneracy. The linear dependence of states' energies near the intersection gives rise to singularity points on adiabatic PESs. More precisely, the theorem states that for any geometry with symmetry required degeneracy between the electronic states there exists a nuclear displacement along which the linear derivative coupling matrix element between the unperturbed states and the difference between the diagonal matrix elements of the perturbation *are not required to be zero* by symmetry. The theorem does not guarantee the intersection in real physical problems and the above vibronic terms can become zero due to additional symmetries, properties of the potential, or other reasons. For example, as mentioned in the original paper, the energy splitting can be negligible if the orbital dependence on the displacement is weak, as in the case of lone pairs.

An interesting situation arises when such JT pair interacts with other closely lying states, as it happens in cyclic $N_3^+$. In this case the overall energy dependence at the intersection point becomes purely quadratic and high symmetry configurations can become stationary points on adiabatic PESs.

In triatomics, degenerate PESs usually form a conical intersection (CI) extensively characterized over the years for a variety of systems.[4,5] An important feature of such intersection is that the real electronic wave function calculated within the Born-Oppenheimer approximation gains a phase, i.e., a sign change, along any path on the PES, which encircles a conical intersection and thus contains the singularity point.[6–9] This geometric phase has a profound effect on the nodal structure of the vibrational wave functions, the order of vibrational states, and the selection rules for the vibrational transitions.[10,11]

A common motif in these systems is an unpaired electron in one of the doubly degenerate molecular orbitals (MOs) in the ground electronic state. Alternatively, CIs can be formed by the excited states derived from electron transitions between doubly degenerate and non-degenerate orbitals, e.g., nondegenerate highest occupied molecular orbital (HOMO) and doubly degenerate lowest unoccupied molecular orbital (LUMO) in $NO_3$.

Similar to many other $X_3$ systems, the cyclic $N_3$ radical features CI in the ground state,[12] with unusually strong geometric phase effect that changes the nodal structure of the vibrational wave function and the ordering of vibrational levels.[11]

Cyclic $N_3$ was described as a metastable molecule ten years ago,[13] which was confirmed by later calculations.[14,15] The first experimental evidence of cyclic $N_3$ was obtained by Wodtke and co-workers,[16–18] who reported the cyclic $N_3$ production in the $ClN_3$ photodissociation and measured its ion-

[a)]Electronic mail: krylov@usc.edu

 

ization threshold.[18] These experiments motivated recent theoretical studies of $N_3$, as well as the present work targeting the cyclic $N_3^+$ ground and excited states, in order to facilitate the interpretation of photoelectron experiments. In contrast to the neutral, only limited information is available about the cation states.[19]

The cyclic $N_3$ cation is a closed shell molecule of $D_{3h}$ symmetry with doubly degenerate HOMO and LUMO. Thus, the lowest excited states of each multiplicity are almost quadruply degenerate (with two exactly degenerate states) and exhibit JT-like behavior.

A similar quadruple set of the excited states occurs in other systems with doubly degenerate HOMO and LUMO, for example, in benzene,[20] a rather popular JT system. Interestingly enough, most theoretical studies of the JT effects in benzene were focused on the benzene cation, which exhibits the usual JT conical intersection. As for the neutral molecule, most of the computational studies reported only the vertical excitation energies[21,22] for these four almost degenerate excited states.

The effect of other closely lying electronic states on JT intersections has been discussed by several researchers.[23–25] For example, Perrin and Gouterman[23] analyzed the $(E+A)\otimes e$ vibronic coupling problem. In their treatment, degenerate $E$ states that form CI were considered not as isolated states (e.g., as in the $E\otimes e$ vibronic coupling problem[26]) but as being coupled to a closely lying $A$ state. Similar interactions were characterized in $Na_3$,[24] where the interpretation of the experimental data required the inclusion of the nondegenerate $A_1$ state and treating all three states as a pseudo-Jahn-Teller system.

This work presents a comprehensive analysis of the cyclic $N_3^+$ excited states. We found that two HOMO→LUMO exactly degenerate states do not form a familiar $A_2/B_1$ conical intersection because of the presence of the two other closely lying HOMO→LUMO states of the $A_2$ and $B_1$ symmetries. Nondegenerate states are coupled to the degenerate ones forming an $(E+A+B)\otimes e$ vibronic problem, and the energy dependence on the displacement from the intersection becomes purely quadratic, except for the points of an accidental degeneracy of three states. Such glancing intersection is similar to Renner-Teller glancing intersections in linear molecules.[27] It exhibits pseudo-Jahn-Teller distortions, as opposed to CI and the usual JT effect characterized by the linear dependence of the energy along the displacements, and has no geometric phase effect in the electronic wave functions.[7]

The structure of the paper is as follows. The next section describes computational details. Molecular orbital framework and the nature of low-lying states is presented in Secs. III and IV, respectively. The formal analysis of the $(E+A+B)\otimes e$ JT problem is presented in Sec. V. Section VI discusses ionization potential and photoelectron spectrum. Our final remarks are given in Sec. VII.

## II. COMPUTATIONAL DETAILS

Excited state equilibrium geometries, frequencies, and vertical and adiabatic excitation energies were calculated at the EOM-CCSD (Refs. 28 and 29)/cc-pVTZ (Ref. 30) level of theory with frozen $1s$ core orbitals. Potential energy surfaces of the excited states were obtained at the EOM-CCSD level with the 6-311G* (Ref. 31) basis set. EOM-CCSD/cc-pVTZ PESs presented in this work will be discussed in more detail elsewhere.[32] The ground state of cyclic $N_3^+$ was characterized using the CCSD model with perturbative triples corrections, CCSD(T),[33] and the cc-pVTZ (Ref. 30) basis set.

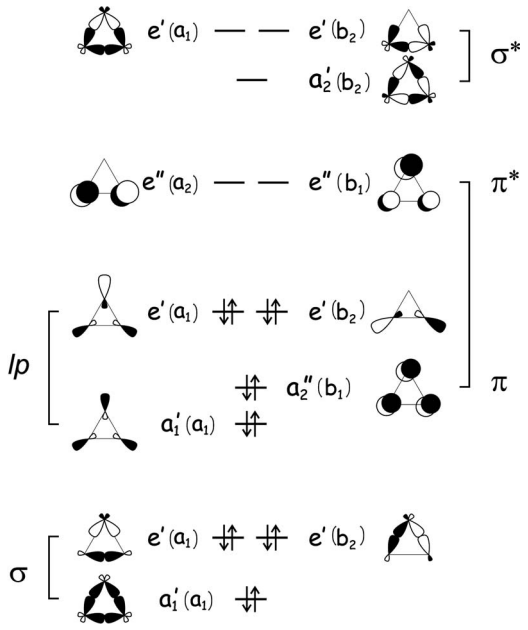


FIG. 1. Molecular orbitals and the ground state electronic configuration of cyclic $N_3^+$ (equilateral triangle, $D_{3h}$). Both HOMO and LUMO are doubly degenerate. $C_{2v}$ labels are given in parentheses.

The ionization potential of cyclic $N_3$ was calculated as the energy difference between the neutral and the cation using the CCSD(T) total energies with the following bases:[30] cc-pVDZ→cc-pVTZ→cc-pVQZ→cc-pV5Z ($1s$ core orbitals were frozen). The three latter basis sets were used for the three point basis set extrapolation CBS-3pa (Refs. 34 and 35) of the neutral and cation total energies,

$$E_{\text{cc-pV}XZ}(X) = E_{\text{BSL}} + be^{-cX},$$

where $E_{\text{cc-pV}XZ}$ is the total energy obtained with cc-pV$XZ$ basis set, $X$ denoting a cardinal number: $X=\{\text{T},\text{Q},5\}$, $E_{\text{BSL}}$ is the extrapolated basis set limit energy, and $b$ and $c$ are the fitting constants. The EOM-SF-CCSD (Refs. 36 and 37)/cc-pVTZ equilibrium geometry of the neutral cyclic $N_3$ and the CCSD(T)/cc-pVTZ equilibrium geometry of the cation were used in the IP calculations. The zero point energy (ZPE) of neutral cyclic $N_3$ including the geometric phase effect is from Ref. 11. Cation's ZPE is calculated at the harmonic approximation at the CCSD(T)/cc-pVTZ level of theory.

EOM-EE-CCSD and EOM-SF-CCSD results were obtained with the Q-CHEM (Ref. 38) *ab initio* package. CCSD(T) calculations were performed with the ACES II (Ref. 39) electronic structure program.

## III. MOLECULAR ORBITAL PICTURE

The ground state equilibrium geometry of cyclic $N_3^+$ is an equilateral triangle ($D_{3h}$) with $R_{NN}=1.313$ Å. Figure 1 shows

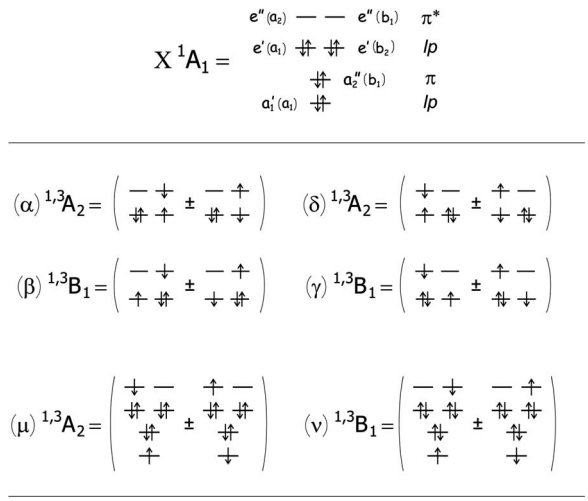


FIG. 2. Leading electronic configurations of the ground (top panel) and the lowest excited states (lower panel). HOMO→LUMO excitations give rise to four singlet and four triplet CSFs labeled $\alpha$, $\beta$, $\gamma$, and $\delta$. HOMO-2 →LUMO excitations yield two additional CSFs of each multiplicity: ($\mu$) and ($\nu$).

MOs and the ground sate electronic configuration of $N_3^+$, which is a closed shell molecule with $A_1'$ ($A_1$ in $C_{2v}$) electronic wave function. MOs are derived from: (i) the $sp^2$ hybridized $2s$, $2p_x$, and $2p_y$ atomic orbitals, which form nine molecular orbitals—three $\sigma$-bonding, three $\sigma$-antibonding ($\sigma^*$), and three lone pair ($lp$) orbitals, and (ii) $2p_z$ atomic orbitals that form three $\pi$-like MOs. Each triple set of MOs (i.e., $\sigma$, $\sigma^*$, $lp$, or $\pi$) exhibits a similar pattern—one fully bonding MO lies bellow two exactly degenerate orbitals. There is no clear energy separation between the $\pi$ and $lp$ sets. An interesting feature of this molecule is that both HOMO and LUMO are doubly degenerate. HOMOs ($lp$'s) are of $e'$ symmetry, whereas LUMOs ($\pi^*$) are of $e''$ symmetry. At $C_{2v}$, the HOMO pair splits into $a_1$ and $b_2$, and LUMO—into the $a_2$ and $b_1$ orbitals.

## IV. LOWEST EXCITED STATES

The least symmetric configuration of a triangular molecule is $C_s$. We use $C_{2v}$ symmetry labels for the twelve lowest excited states, which all are of either $A_2$ or $B_1$ symmetry and therefore become $A''$ at $C_s$. $D_{3h}$ labels are also given when appropriate.

Figure 2 shows leading configurations of the ground and the lowest excited states. Different determinants are combined in configuration state functions (CSFs) that have appropriate spin and spatial symmetry and represent a convenient basis for describing excited states.

The lowest excited states of cyclic $N_3^+$ are derived from the eight possible single excitations from doubly degenerate HOMO to doubly degenerate LUMO ($lp \rightarrow \pi^*$, top panel). The symmetries of respective CSFs are given by $(a_1+b_2) \otimes (a_2+b_1)=(A_2+A_2+B_1+B_1)$, and each of these can be either a singlet or a triplet. Thus, a total of eight different CSFs can be formed, as shown in Fig. 2 (lower panel). Labels $\alpha$, $\beta$, $\gamma$, and $\delta$ denote different types of CSF, whereas minus or plus signs correspond to singlet or triplet configurations, respectively. Next two singlets and triplets ($\mu$ and $\nu$) are derived from the excitations from nondegenerate HOMO-2 to LUMO.

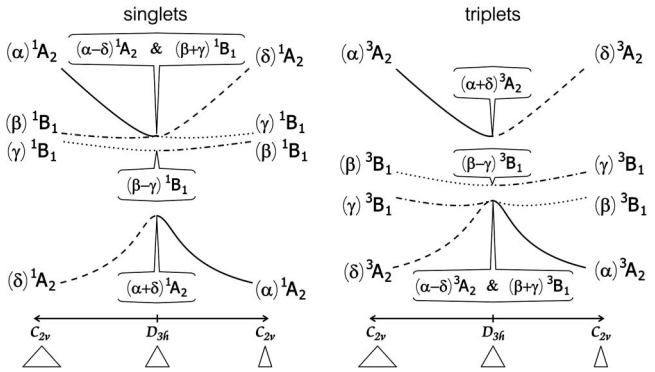


FIG. 3. Changes in the excited states' characters and potential energy surfaces upon distortions from an equilateral ($D_{3h}$) geometry to an obtuse (left) and an acute (right) isosceles $C_{2v}$ triangles.

Only CSFs of the same spin and irrep can mix in the excited state wave functions. For example, two singlet $A_2$ states are described as linear combinations of two singlet $A_2$ CSFs,

$$|(\alpha+\delta)\ ^1A_2\rangle = \frac{1}{\sqrt{\kappa^2+\lambda^2}}[\kappa \cdot |(\alpha)\ ^1A_2\rangle + \lambda \cdot |(\delta)\ ^1A_2\rangle]$$

$$|(\alpha-\delta)\ ^1A_2\rangle = \frac{1}{\sqrt{\kappa^2+\lambda^2}}[\lambda \cdot |(\alpha)\ ^1A_2\rangle - \kappa \cdot |(\delta)\ ^1A_2\rangle] \quad (1)$$

The wave functions of two triplet $|(\alpha\pm\delta)\ ^3A_2\rangle$ states can be formed in a similar way. Likewise, four $B_1$ states (two singlets and two triplets) $|(\beta\pm\gamma)B_1\rangle$ are linear combinations of $|(\beta)B_1\rangle$ and $|(\gamma)B_1\rangle$ CSFs. The coefficients $\kappa$ and $\lambda$ are both equal to one at $D_{3h}$, whereas along $C_{2v}$ distortions (e.g., along the bending normal mode) their ratio changes. In other words, at $D_{3h}$ the excited state wave functions are simply a sum or a difference of basis CSFs, and a $C_{2v}$ distortion collapses each state into single CSF (see Fig. 3). Thus, these CSFs represent an approximate diabatic basis. Overall, at $D_{3h}$ geometries four singlet and four triplet excited state wave functions are formed from four CSFs with $\lambda=\kappa=1$: $|(\alpha+\delta)\ ^{1,3}A_2\rangle$, $|(\alpha-\delta)\ ^{1,3}A_2\rangle$, $|(\beta+\gamma)\ ^{1,3}B_1\rangle$, and $|(\beta-\gamma)\ ^{1,3}B_1\rangle$. Since all CSFs are derived from the single excitations between the two pairs of doubly degenerate orbitals, the resulting states are also nearly degenerate and form a rather complicated $D_{3h}$ intersection. The $|(\mu)\ ^{1,3}A_2\rangle$ and $|(\nu)\ ^{1,3}B_1\rangle$ states derived from HOMO-2→LUMO excitations do not mix at $D_{3h}$ geometry and form a regular JT pair.

Using $D_{3h}$ symmetry labels, the symmetries of the HOMO→LUMO states are

$$e' \otimes e'' \rightarrow A_1'' + A_2'' + (E'') \xrightarrow{C_{2v}} A_2 + B_1 + (A_2 + B_1), \quad (2)$$

i.e., among these four excited states only one $A_2$ and one $B_1$ state are exactly degenerate $E''$ states forming a JT pair.

TABLE I. Vertical excitation energies (eV) of the 12 lowest excited states of cyclic $N_3^+$ calculated at the EOM-CCSD/cc-pVTZ level of theory. Two out of four HOMO→LUMO ($\alpha-\delta$, $\beta+\gamma$) and two HOMO-2→LUMO ($\mu$, $\nu$) excited states are exactly degenerate pairs at $D_{3h}$. The ground state geometry and total energy are given in Table II.

| Singlets | | Triplets | |
|---|---|---|---|
| $(\nu)\ ^1A_2$ | 7.669 | $(\nu)\ ^3A_2$ | 7.014 |
| $(\mu)\ ^1B_1$ | 7.669 | $(\mu)\ ^3B_1$ | 7.014 |
| $(\alpha-\delta)\ ^1A_2$ | 5.334 | $(\alpha+\delta)\ ^3A_2$ | 4.333 |
| $(\beta+\gamma)\ ^1B_1$ | 5.334 | | |
| | | $(\beta-\gamma)\ ^3B_1$ | 3.950 |
| $(\beta-\gamma)\ ^1B_1$ | 5.314 | | |
| | | $(\beta+\gamma)\ ^3B_1$ | 3.921 |
| $(\alpha+\delta)\ ^1A_2$ | 4.914 | $(\alpha-\delta)\ ^3A_2$ | 3.921 |

These degenerate states are $|(\alpha-\delta)A_2\rangle$ and $|(\beta+\gamma)B_1\rangle$. HOMO-2→LUMO states, $(\mu)\ ^{1,3}A_2$ and $(\nu)\ ^{1,3}B_1$, form another $E'$ JT pair. Calculated vertical excitation energies for the 12 lowest excited states are summarized in Table I. As explained above, only two of the four HOMO-LUMO states are exactly degenerate; however, the order of the states is different for singlets and triplets.

PES scans along the bending normal coordinate are shown in Fig. 4 separately for each irrep and multiplicity. The coordinate origin ($Q_b=0.0$) corresponds to $N_3^+$ at the equilateral $D_{3h}$ geometry ($R_{NN}=1.313$ Å), whereas left and right wings of the plots correspond to $C_{2v}$ distortions. The scale along the bending normal mode is as follows: $Q_b=0.4$ corresponds to $\theta=45.3°$ and $R_{NN}=1.430$ Å, whereas $Q_b=-0.4$—to $\theta=77.2°$ and $R_{NN}=1.220$ Å.

The ground $X\ ^1A_1$ state, which has $D_{3h}$ equilibrium geometry, is shown by the solid line and empty circles on each plot. The lowest excited states (filled squares, triangles, and circles) have singly occupied degenerate orbitals and undergo JT distortions to $C_{2v}$.

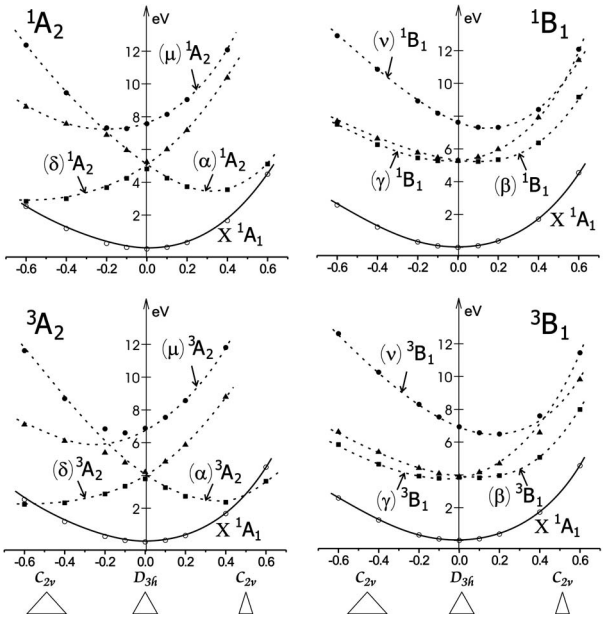


FIG. 4. The EOM-CCSD/6-311G* potential energy surface scans along the bending normal coordinate for the ground ($X\ ^1A_1$, shown on each plot) and the excited $^1A_2$, $^1B_1$, $^3A_2$, $^3B_1$ states of cyclic $N_3^+$ (upper left, upper right, lower left, and lower right, respectively). Data points (squares, triangles, and filled circles) correspond to the calculated adiabatic surfaces; dashed lines represent approximate diabats and connect points with the same leading character of the wave function (see Fig. 2).

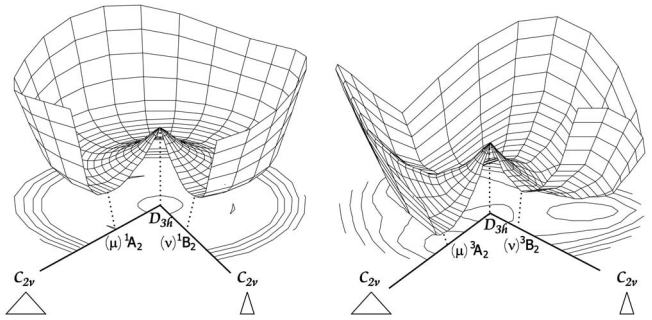


FIG. 5. Adiabatic potential energy surfaces and contour plots of the $(\mu)A_2$ and $(\nu)B_1$ singlet (left) and triplet (right) states. Polar radius and angle are hyperspherical coordinates $\theta$ and $\phi$, which are similar to the bending and asymmetric stretch normal mode, respectively. Stereographic projection is taken with fixed hyperradius (overall molecular size or symmetric stretch) $\rho=3.262$ corresponding to the cyclic $N_3^+$ ground state equilibrium geometry. Both surfaces feature conical $(\mu)A_2/(\nu)B_1$ intersection at $D_{3h}$. Stationary points on the surfaces are located along two $C_{2v}$ distortions to acute and obtuse isosceles triangles. Energies of the transition state and the conical intersection relative to the minima are $E_{TS}=0.05$ eV, $E_{CI}=0.97$ eV and $E_{TS}=0.24$ eV, $E_{CI}=1.03$ eV on the singlet and tiplet $(\mu/\nu)$ PESs, respectively.

Let us first discuss the $(\mu)\ ^{1,3}A_2$ and $(\nu)\ ^{1,3}B_1$ states derived from the excitations from nondegenerate HOMO-2 to doubly degenerate LUMO (two lowest CSFs in Fig. 2). These states are shown in the each plot in Fig. 4 by the very top dashed line. The two singlets, $(\mu)\ ^1A_2$ and $(\nu)\ ^1B_1$, are exactly degenerate at $D_{3h}$ and undergo JT distortions to $C_{2v}$. The stereographic projections of PESs using hyperspherical coordinates[40] of PESs shown in Fig. 5 reveal the similarity of this intersection to the $^2B_1/^2A_2$ intersection in neutral cyclic $N_3$.[11] Transition from the acute to the obtuse triangle stationary points through the $D_{3h}$ point (i.e., along the bending normal mode) encounters a relatively high potential barrier; however, the molecule can go around the conical intersection with almost no barrier following the asymmetric normal mode that corresponds to pseudorotation. The seam of this conical intersection is along the fully symmetric stretch. The pair of the $(\mu)^3A_2$ and $(\nu)^3B_1$ triplet states follows the same pattern, although the energy differences between the respective equilibrium geometries (EG) and the transition states (TS) are slightly larger (see Table II), and the barrier for pseudorotation is higher. Such $A_2/B_1$ intersection causes the electronic wave function to gain a phase (change of a sign) along any path on the adiabatic PES that encircles CI.[11]

The four lower excited states ($\alpha$, $\beta$, $\gamma$, and $\delta$) show a different and more complicated behavior, due to the double degeneracy of initial and target MOs (Fig. 2). Instead of a JT pair, they form a JT quartet: four almost degenerate electronic states, which are all unstable at $D_{3h}$ and distort to lower symmetries. The calculated PES of this intersection is presented in Fig. 6, and the excited state characters around the intersection point are sketched in Fig. 3 (see also PES

TABLE II. $C_{2v}$ constrained optimized geometries, harmonic vibrational frequencies, and total ($E_{tot}$) and adiabatic excitation ($E_{ex}$) energies of the ground ($X\,^1A_1$) and the lowest excited states calculated at the EOM-CCSD/cc-pVTZ level of theory. $\omega_1$, $\omega_2$, and $\omega_3$ are the frequencies of the symmetric stretch, bending, and asymmetric stretch, respectively.

| | $X\,^1A_1$ | $(\alpha)\,^1A_2$ | $(\beta)\,^1B_1$ | $(\gamma)\,^1B_1$ | $(\delta)\,^1A_2$ | $(\mu)\,^1A_2$ | $(\nu)\,^1B_1$ |
|---|---|---|---|---|---|---|---|
| $E_{ex}$ (eV) | 0.00 | 2.92 | 5.16 | 5.19 | 2.51 | 6.76 | 6.81 |
| $E_{tot}$ (a.u.) | −163.423 29 | −163.315 93 | −163.233 79 | −163.232 66 | −163.331 06 | −163.174 96 | −163.172 89 |
| $\theta$ (°) | 60.0 | 37.7 | 56.0 | 62.1 | 92.2 | 52.3 | 66.3 |
| $R_{NN}$ (Å) | 1.313 | 1.750 | 1.389 | 1.343 | 1.244 | 1.475 | 1.365 |
| $E_{nuc}$ (a.u.) | 59.237 38 | 55.523 43 | 57.234 05 | 57.328 02 | 56.139 34 | 55.077 21 | 55.364 57 |
| $\omega_1$ ($cm^{-1}$) | 1646 | 2134 | 1427 | 1401 | 1633 | | |
| $\omega_2$ ($cm^{-1}$) | 1108 | 363 | 823 | 1013 | 597 | n/a[b] | n/a[b] |
| $\omega_3$ ($cm^{-1}$) | 1108 | $-i424$ | 1163 | $-i1362$ | 764 | | |
| ZPE (kcal/mol) | 5.521 | 3.830[a] | 4.880 | 3.451[a] | 4.280 | | |
| | | $(\alpha)\,^3A_2$ | $(\beta)\,^3B_1$ | $(\gamma)\,^3B_1$ | $(\delta)\,^3A_2$ | $(\mu)\,^3A_2$ | $(\nu)\,^3B_1$ |
| $E_{ex}$ (eV) | | 1.15 | 3.85 | 3.82 | 1.94 | 6.04 | 6.28 |
| $E_{tot}$ (a.u.) | | −163.380 90 | −163.281 92 | −163.283 07 | −163.352 13 | −163.201 32 | −163.192 52 |
| $\theta$ (°) | | 34.1 | 57.0 | 63.3 | 90.9 | 51.9 | 64.4 |
| $R_{NN}$ (Å) | | 1.910 | 1.360 | 1.322 | 1.249 | 1.473 | 1.372 |
| $E_{nuc}$ (a.u.) | | 50.334 01 | 58.090 07 | 57.906 82 | 56.091 25 | 55.332 35 | 55.522 38 |
| $\omega_1$ ($cm^{-1}$) | | 2241 | 1429 | 1419 | 1603 | 2701 | 1751 |
| $\omega_2$ ($cm^{-1}$) | | 434 | 889 | 999 | 599 | 1129 | 1361 |
| $\omega_3$ ($cm^{-1}$) | | $-i385$ | $-i1010$ | 1470 | $-i1366$ | 1514 | $-i1669$ |
| ZPE, kcal/mol | | 3.570[a] | 3.313[a] | 5.558 | 3.148[a] | 7.639 | 4.450[a] |

[a]ZPE for the transition states were calculated only for normal coordinates with real frequencies, i.e., bending and symmetric stretch.
[b]We were not able to calculate frequencies for the ($\mu$) and ($\nu$) states because of the numerical instability of finite difference procedure in the vicinity of the conical intersection.

cuts along $C_{2v}$ distortions in Fig. 4). Obviously, this is not a quadruply degenerate intersection—only two out of the four electronic states are exactly degenerate at $D_{3h}$, as described above. Nevertheless, all four states around the intersection strongly interact, which results in a fascinating pattern. For example, the intersection of the two degenerate states is *glancing* rather than *conical*, and the energy depends only quadratically on the displacements from the intersection point,[6,7] as explained in detail in Sec. V. Note that the singlets (left panel, Fig. 3) form almost a triply degenerate intersection: $(\beta-\gamma)\,^1B_1$ state is only 0.02 eV (Table I) lower than the $(\alpha-\delta)\,^1A_2/(\beta+\gamma)\,^3B_1$ pair. Interestingly, the order and the character of the excited states at $D_{3h}$ is different for singlets and triplets, although it becomes the same for the geometries distant from the equilateral triangle as shown by the labels on the left and right sides of the plots in Fig. 3.

The intersection topology is further clarified by the additional scan along the fully symmetric stretch normal bond $Q_{ss}$ that corresponds to changing the overall size of the equilateral triangle (Fig. 7). All four states of each multiplicity remain close in energy along $Q_{ss}$, and the two exactly degenerate states retain their degeneracy (solid line in Fig. 7) forming the seam of the glancing intersection. However, the nondegenerate states (filled circles and squares) slightly change their energy position relative to the glancing intersection, which changes the order of the triplet states and even leads to additional accidental degeneracies of the $(\alpha+\delta)\,^3A_2$ or $(\beta-\gamma)\,^3B_1$ states with the glancing intersection at some $D_{3h}$ geometries (encircled in Fig. 7).

Optimized geometries, frequencies, and adiabatic excitation energies of the excited states described above are presented in Table II. As in many JT triatomics, one sheet of $(\beta)/(\gamma)$ singlet and triplet PESs has a minimum (EG), and another—a transition state, the later corresponding to the potential barrier for pseudorotation motion between the equivalent EG minima. $(\alpha)/(\delta)$ states could follow the similar pattern; however, the $(\alpha)$ singlet and triplet states are dissociative along the $C_{2v}$ distortion. If the $C_{2v}$ constrain is lifted, the $(\alpha)$ states relax to linear structures: the $(\alpha)\,^1A_2$ assumes $C_{\infty v}$ geometry with $R_{NN}=1.178$ Å, whereas the triplet $(\alpha)\,^3A_2$ becomes $D_{\infty h}$ with $R_{12}=1.123$ Å and $R_{23}=1.279$ Å.

The shape of the $\alpha/\delta$ and $\beta/\gamma$ PES crossings is different from that of $\mu/\nu$ CI (and also from the $^2B_1/^2A_2$ intersection in neutral cyclic $N_3$), as the surfaces $\alpha/\delta$ and $\beta/\gamma$ have only a quadratic dependence on a displacement from the intersection point. Thus, even though there are two exactly degenerate JT states, the intersection is glancing rather than conical and adiabatic PESs do not have singularities.

This changes the behavior of electronic wave function in the vicinity of the intersection: although the character of the electronic wave function changes along the path around the intersection, the point group symmetry remains the same, and, therefore, the electronic wave function does not gain a sign change. Thus, there is no geometric phase effect along any path that stays on one of the four adiabatic PESs and encircles this intersection,[6,7] which is not surprizing, in view of the absence of a singularity point.

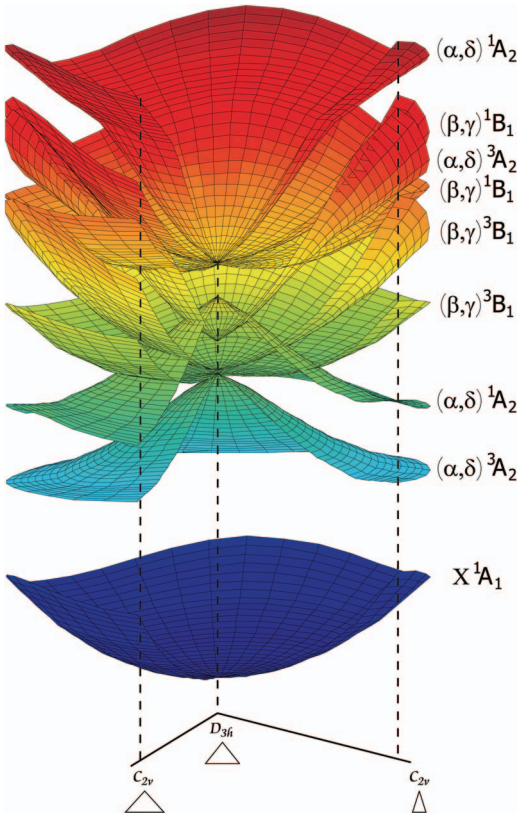


FIG. 6. (Color) PESs of the ground ($X$) and the first eight excited states of cyclic $N_3^+$. Coordinates are as in Fig. 5. Three out of four states in each multiplicity are almost degenerate at $D_{3h}$ geometry, two being exactly degenerate.

## V. THE ANALYSIS OF THE $(E+A+B)\otimes E$ PROBLEM IN CYCLIC $N_3^+$

The electronic Hamiltonian $H=T_e+U(\mathbf{r},\mathbf{Q})$ can be expanded as Taylor series with respect to small nuclear displacements $Q\rho$ from a reference high symmetry configuration $(Q_\rho=0)$,

$$H = H^0 + \sum_\rho \frac{\partial H}{\partial Q_\rho} Q_\rho + \sum_{\rho,\sigma} \frac{\partial^2 H}{\partial Q_\rho \partial Q_\sigma} Q_\rho Q_\sigma + \ldots = H^0 + V. \tag{3}$$

We truncate this expansion at linear terms and start by solving the Schrödinger equation for Hamiltonian $H^0$. The perturbation $V$ thus includes linear vibronic coupling terms $\Sigma_\rho(\partial H/\partial Q_\rho)Q_\rho$.[1,2]

Instead of taking eigenfunctions of $H^0$ as a basis set for a subsequent perturbative treatment, we choose to employ a diabatic basis of HUMO→LUMO CSFs (see Fig. 2). These CSFs are close to adiabatic states for $C_{2v}$ distorted geometries, whereas at $D_{3h}$ $(Q_\rho=0)$ the corresponding adiabatic states (i.e., eigenstates of $H^0$) are the linear combinations of CSFs, as given by Eq. (1).

We employ normal coordinates: bending $Q_b$, asymmetric stretch $Q_{\text{as}}$ and symmetric stretch $Q_{\text{ss}}$, which are of $a_1$, $b_2$, and $a_1$ symmetry (in $C_{2v}$), respectively. We will consider $Q_b$ and $Q_{\text{as}}$, which constitute the $e'$ degenerate vibration. The third normal coordinate $Q_{\text{ss}}$ describes breathing motion, which does not lift the degeneracy between MOs and CSFs. This mode will be discussed in the end of the section.

The matrix elements $V_{ij}$ of the vibronic coupling term are

$$V_{ij} = \langle \Psi_i | \sum_\rho \frac{\partial H}{\partial Q_\rho} Q_\rho | \Psi_j \rangle = \sum_\rho \langle \Psi_i | \frac{\partial U}{\partial Q_\rho} | \Psi_j \rangle Q_\rho = \sum_\rho F_{ij}^{Q_\rho} Q_\rho, \tag{4}$$

where $\{\Psi_k\}$ are the diabatic $\{(\alpha)A_2,(\delta)A_2,(\beta)B_1,(\gamma)B_1\}$ basis functions.

Selection rules for $F_{ij}^{Q_\rho}$,[41] derivative or linear vibronic coupling constant, are readily derived from the group theory considerations. $V_{ij}$ is nonzero only if $\Gamma_{\langle i|}\otimes\Gamma_{Q_\rho}\otimes\Gamma_{|j\rangle}$ includes totally symmetric irrep $A_1$, where $\Gamma_{\langle i|}$, $\Gamma_{|j\rangle}$, and $\Gamma_{Q_\rho}$ are the irreps of the $\Psi_i$, $\Psi_j$ diabats and the $Q_\rho$ normal mode, respectively. Thus, the linear vibronic coupling is nonzero between the states of the same symmetry only along the bending normal coordinate, e.g., $\Gamma_{\langle B_1|}\otimes\Gamma_{Q_b(a_1)}\otimes\Gamma_{|B_1\rangle}\supset A_1$. For the states of different symmetry, i.e., $A_2$ and $B_1$, it is nonzero only along the asymmetric stretch: $\Gamma_{\langle A_2|}\otimes\Gamma_{Q_{\text{as}}(b_2)}\otimes\Gamma_{|B_1\rangle}\supset A_1$. Thus, the vibronic coupling matrix elements $V_{ij}$ are

$$\begin{aligned}
\langle \Psi_i^{A_2} | V | \Psi_j^{A_2} \rangle &= F_{ij}^{Q_b} Q_b, \\
\langle \Psi_i^{B_1} | V | \Psi_j^{B_1} \rangle &= F_{ij}^{Q_b} Q_b, \\
\langle \Psi_i^{B_1} | V | \Psi_j^{A_2} \rangle &= F_{ij}^{Q_{\text{as}}} Q_{\text{as}}.
\end{aligned} \tag{5}$$

The $H^0$ off-diagonal matrix elements are nonzero only between the states of the same symmetry,

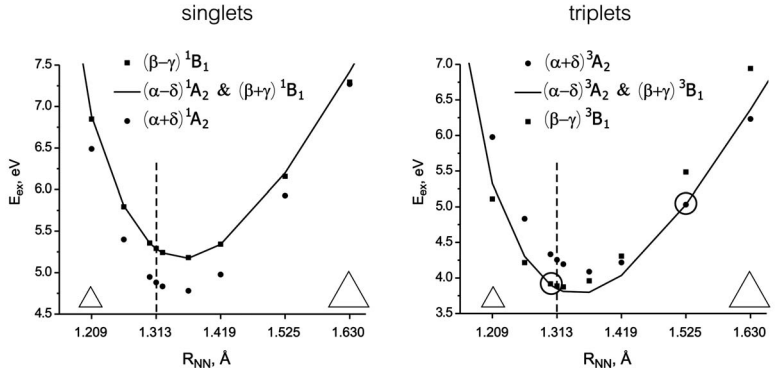


FIG. 7. EOM-CCSD/6-311G* potential energy surface scans along symmetric stretch normal coordiante for the lowest $A_2$ and $B_1$ excited states. Singlets are shown on the left plot, triplets—on the right. Solid line shows two exactly degenerate states the $(\alpha-\delta)A_2$ and $(\beta+\gamma)B_1$, i.e., the seam of the intersection. Circles and squares correspond to the nondegenerate $(\alpha+\delta)A_2$ and $(\beta-\gamma)B_1$ states, respectively. Big circles on the right plot show two tree-state PES intersections. $R_{NN}$ is a bond length of equilateral triangle, vertical dashed line points at the cyclic $N_3^+$ ground state equilibrium geometry.

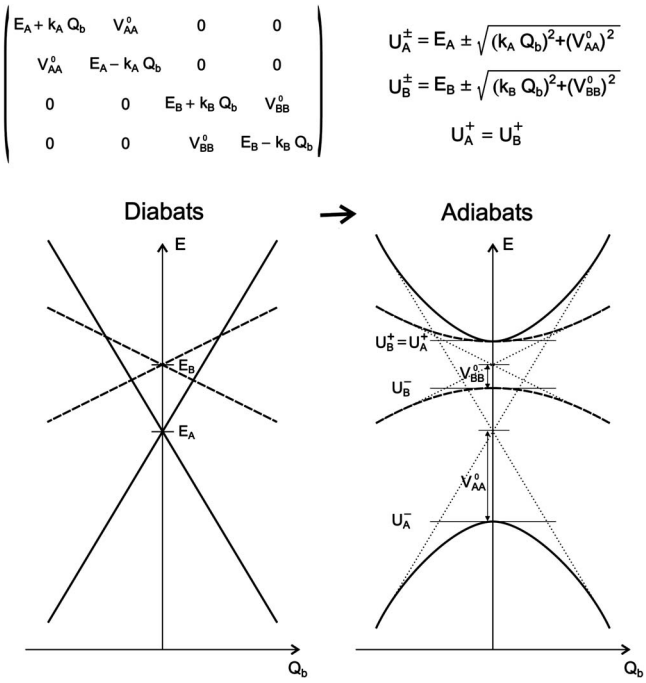


FIG. 8. The Hamiltonian in the diabatic (left) and adiabatic (right) representations along the bending normal mode $Q_b$. Since the Hamiltonian is block diagonal, the pairs of states of the same symmetry do not interact with each other and form two noncrossing pairs (see text).

$$\langle \Psi_i^{A_2} | H^0 | \Psi_j^{A_2} \rangle = V_{AA}^0,$$

$$\langle \Psi_i^{B_1} | H^0 | \Psi_j^{B_1} \rangle = V_{BB}^0, \tag{6}$$

$$\langle \Psi_i^{B_1} | H^0 | \Psi_j^{A_2} \rangle = 0.$$

Using Eqs. (5) and (6), the Hamiltonian in the diabatic basis set $\{(\alpha)A_2, (\delta)A_2, (\beta)B_1, (\gamma)B_1\}$ assumes the following form:

$$H(Q_b, Q_{\mathrm{as}}) = \begin{pmatrix} E_A + k_A Q_b & V_{AA}^0 & F_{\alpha\beta} Q_{\mathrm{as}} & F_{\alpha\gamma} Q_{\mathrm{as}} \\ V_{AA}^0 & E_A - k_A Q_b & F_{\delta\beta} Q_{\mathrm{as}} & F_{\delta\gamma} Q_{\mathrm{as}} \\ F_{\alpha\beta} Q_{\mathrm{as}} & F_{\delta\beta} Q_{\mathrm{as}} & E_B + k_B Q_b & V_{BB}^0 \\ F_{\alpha\gamma} Q_{\mathrm{as}} & F_{\delta\gamma} Q_{\mathrm{as}} & V_{BB}^0 & E_B - k_B Q_b \end{pmatrix}, \tag{7}$$

where $k_A = F_{\alpha\alpha}^{Q_b} = -F_{\delta\delta}^{Q_b}$ and $k_B = F_{\beta\beta}^{Q_b} = -F_{\gamma\gamma}^{Q_b}$.

Along the bending normal mode $Q_b$, when $Q_{\mathrm{as}}=0$, CSFs of different symmetries are not coupled, and the Hamiltonian (7) assumes a block diagonal form. Thus, pairs $\{(\alpha)A_2, (\delta)A_2\}$ and $\{(\beta)B_1, (\gamma)B_1\}$ form two pairs of noncrossing adiabats (see Fig. 8, compare to Fig. 3).

At $D_{3h}$, i.e., when $Q_b=0$ and $Q_{\mathrm{as}}=0$, it is required by symmetry, Eq. (2), that one of the $A_2$ states ($U_A^{\pm}$) is degenerate with one of the $B_1$ states ($U_B^{\pm}$), i.e., in the example shown in Fig. 8 the intersection condition is $U_A^+ = U_B^+$, which gives rise to the additional condition $E_A + |V_{AA}^0| = E_B + |V_{BB}^0|$. By shifting the energy scale such that one of the diabatic energies at the intersection is zero, this condition becomes

$$|V_{BB}^0| = |V_{AA}^0| - E_B,$$
$$E_A = 0. \tag{8}$$

The coupling between the two degenerate states at ($Q_b=0$, $Q_{\mathrm{as}}=0$) is zero by virtue of Eqs. (5) and (6). Thus, the derivatives of the potential energy surfaces ($U_i$) along the bending coordinate (see Fig. 8) are zero,

$$\left. \frac{\partial U_i}{\partial Q_b} \right|_{Q_{\mathrm{as}}=Q_b=0} = 0, \quad i = 1 \ldots 4, \tag{9}$$

which means that the linear terms are absent and the intersection is glancing rather than conical.

The Hamiltonian along the asymmetric stretch $Q_{\mathrm{as}}$ is obtained from matrix (7) by using $Q_b=0$ and condition (8). If only two intersecting states are considered, the problem is similar to the familiar conical intersection[4,5] of $E''$ degenerate states,

$$H = \begin{pmatrix} k_A Q_b & F_{\alpha\beta} Q_{\mathrm{as}} \\ F_{\alpha\beta} Q_{\mathrm{as}} & k_B Q_b \end{pmatrix}. \tag{10}$$

However, because of the two other states $A_2$ and $B_1$, which are almost degenerate with $E''$ pair, the linear vibronic coupling constants $F_{ij}^{Q_{\mathrm{as}}}$ are nonzero and the $4\times4$ full Hamiltonian should be considered at the first order of perturbation theory.

This $4\times4$ problem can be solved analytically, e.g., by using MATHEMATICA.[42] The resulting (rather tedious!) expressions for eigenvalues can be differentiated, which reveals that the eigenvalues' derivatives along the asymmetric stretch coordinate are also zero, similar to the derivatives along $Q_b$. Thus,

$$\left. \frac{\partial U_i}{\partial Q_{\mathrm{as}}} \right|_{Q_{\mathrm{as}}=Q_b=0} = 0, \quad i = 1 \ldots 4, \tag{11}$$

and therefore all four potential energy surfaces ($E''+A_2+B_1$) depend only quadratically on the displacements along the degenerate vibration $e''=Q_b+Q_{\mathrm{as}}$ from $D_{3h}$ geometry, i.e., they have an extremum at the symmetric configuration. Note that the inclusion of the second order terms in the perturbation does not change the derivatives in Eqs. (9) and (11).

Thus, the intersection of four HOMO-LUMO excited states is glancing,[43–45] and all four $(E+A+B)\otimes e$ vibronically coupled states follow a pseudo-Jahn-Teller distortion. Contrary to the conical intersection case, there is no geometric phase effect along any path that encircles the intersection point.[7,24,26]

The absence of linear terms can also be demonstrated by considering $2\times2$ block of the Hamiltonian in the basis of adiabatic JT states (i.e., two degenerate eigenstates of $H^0$), as elegantly shown by Pupyshev.[46] The proof requires the construction of complex $e'$ and $e''$ MOs obtained from $a_1/b_2$ HOMOs and $a_2/b_1$ LUMOs,

$$e'_{\pm} = \frac{1}{\sqrt{2}}(a_1 \pm ib_2),$$

$$e''_{\pm} = \frac{1}{\sqrt{2}}(-b_1 \pm ia_2). \tag{12}$$

In this basis, two degenerate adiabatic states $\Psi_{E_+}$ and $\Psi_{E_-}$ are simply single $e'_+ \rightarrow e''_-$ and $e'_- \rightarrow e''_+$ excitations,

$$\Psi^{1,3}_{E_+} = \frac{1}{\sqrt{2}}(|e'_+\alpha\, e'_-\alpha\, e'_-\beta\, e''_-\beta\rangle \pm |e'_+\beta\, e'_-\alpha\, e'_-\beta\, e''_-\alpha\rangle),$$

$$\Psi^{1,3}_{E_-} = \frac{1}{\sqrt{2}}(|e'_+\alpha\, e'_+\beta\, e'_-\alpha\, e''_+\beta\rangle \pm |e'_+\alpha\, e'_+\beta\, e'_-\beta\, e''_+\alpha\rangle). \tag{13}$$

The above can be derived by either transforming the original adiabatic states into the new MO basis or by symmetry considerations. In terms of diabatic CSFs from Fig. 2, these states are

$$\Psi^{1,3}_{E_\pm} = \frac{1}{\sqrt{2}}[(|(\alpha)A_2\rangle - |(\delta)A_2\rangle) \pm i(|(\beta)B_1\rangle + |(\gamma)B_1\rangle)]. \tag{14}$$

As clearly seen from Eq. (13), $\Psi_{E_+}$ is *doubly excited* with respect to $\Psi_{E_-}$. Neglecting the changes in MOs upon small geometric distortion, the perturbation operator $\partial U/\partial Q$ is a one-particle operator, and, therefore, the corresponding matrix element is zero. There is no linear dependence in $\langle\Psi_{E_\pm}|\partial U/\partial Q_{\rm as}|\Psi_{E_\pm}\rangle$ and $\langle\Psi_{E_\pm}|\partial U/\partial Q_b|\Psi_{E_\pm}\rangle$ diagonal terms because of the symmetry.[46] Note that the double degeneracy of both initial and target MOs (e.g., HOMO and LUMO) is required for the two respective electronic states to be doubly excited with respect to each other. Thus, both proofs show that the cancellation of linear terms occurs due to the presence for of four interacting CSFs.

The change of the overall size of cyclic $N_3^+$ under $D_{3h}$ constraint corresponds to the symmetric stretch (triangle breathing) $Q_{\rm ss}$ $(a1)$ motion, with $Q_b = Q_{\rm as} = 0$. The $E''$ or $A_2 + B_1$ pair of states remains degenerate at any point along $Q_{\rm ss}$. Both zero and first order coupling terms between the states of different symmetries are identically zero by symmetry, which means that the $A_2$ states do not interact with the $B_1$ states along $Q_{\rm ss}$, as well as along the $Q_b$ normal mode of the same $a_1$ symmetry. However, the derivative coupling between two states of the same symmetry, e.g., $|(\alpha)A_2\rangle$ and $|(\delta)A_2\rangle$, is nonzero along the $Q_{\rm ss}$ and can accidentally cancel out the zero order coupling term $V_{AA}$, which results in a triple degeneracy $(E''+A_2)$. By setting $Q_{\rm ss}$ to be equal to zero at such triple degeneracy point and taking into account conditions (8), Hamiltonian (7) assumes the following form:

$$\begin{pmatrix} k_A Q_b & 0 & F_{\alpha\beta}Q_{\rm as} & F_{\alpha\gamma}Q_{\rm as} \\ 0 & -k_A Q_b & F_{\delta\beta}Q_{\rm as} & F_{\delta\gamma}Q_{\rm as} \\ F_{\alpha\beta}Q_{\rm as} & F_{\delta\beta}Q_{\rm as} & E_B + k_B Q_b & -E_B \\ F_{\alpha\gamma}Q_{\rm as} & F_{\delta\gamma}Q_{\rm as} & -E_B & E_B - k_B Q_b \end{pmatrix}. \tag{15}$$

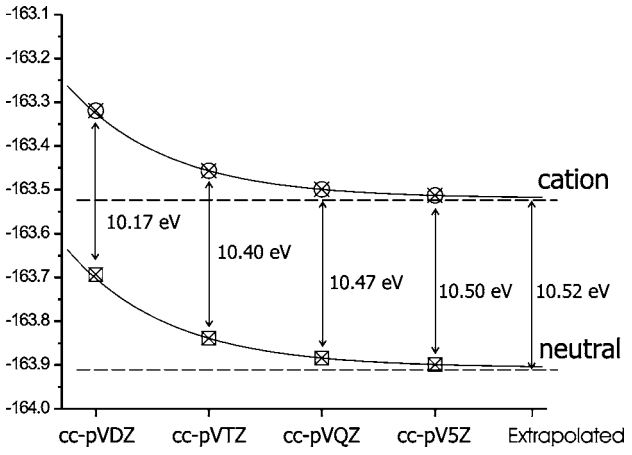


FIG. 9. $IP_{ee}$ (not ZPE corrected) calculated as a difference between neutral's and cation's CCSD(T) total energies in the basis set limit. ZPE corrected IP, $IP_{00}$, is 10.595 eV.

In this case, both derivatives $\partial U_i/\partial Q_b$ and $\partial U_i/\partial Q_{\rm as}$ for $i=1\ldots4$ at $Q_{\rm as}=Q_b=0$ are nonzero, and the intersection has a conical shape in $(Q_{\rm as}, Q_b)$ coordinates: triple conical intersection and a nondegenerate fourth surface with the singularity in the origin $(Q_{\rm as}=0,\ Q_b=0)$. Triple CIs, which are not defined by the high nuclear symmetry, were characterized by Matsika and Yarkony[47,48] as an accidental intersection of two seams of conical intersections. In triatomics, this type of CI was found, for example, in $H_2+H$.[49] In cyclic $N_3^+$, however, the triple CI is formed by two crossing seams of $A''/A''$ conical intersection (in $C_s$) and the $A_2/B_1$ *glancing* intersection (along $D_{3h}$).

To conclude, interactions of a JT pair of states with other states remove linear terms and change the intersection from conical to glancing thus eliminating geometric phase effects.

## VI. IONIZATION POTENTIAL AND PHOTOELECTRON SPECTRUM

The cyclic $N_3^+$ ionization potential was calculated by CCSD(T) with the basis set extrapolation, as described in Sec. II. The results are presented in Fig. 9. Energies of both the neutral and the cation were calculated with four different basis sets. The energy difference extrapolated to the basis set limit is 10.52 eV. The zero point energy (ZPE) of the cation in the harmonic approximation is 0.239 eV (see Table II), and for the neutral cyclic $N_3$ $E$-symmetry vibrational ground state—0.164 eV.[11] Thus, with the ZPE correction, the adiabatic $IP_{00}$ is 10.595 eV. This result supports the experimental measurement of IP for cyclic $N_3^+$ (Ref. 18) of $10.62\pm0.07$ eV.

The IP of the linear $N_3$ radical is 11.06 eV.[50] Therefore, the difference in IPs of the cyclic and linear $N_3$ is only 0.44 eV, which is comparable to the vibrational energy of possibly hot photofragments. Thus, a more detailed analysis of photoelectrons is required to unambiguously assign the observed product as cyclic $N_3$. Below we discuss general features of the cyclic $N_3$ photoelectron spectrum. The calculation of the spectrum and the comparison with the experiments will be reported in a forthcoming paper.[32]

The lowest electronic states of the cation that are bright in a photoelectron experiment are those that are derived from neutral cyclic $N_3$ by one electron ionization: the ground $X\,^1A_1$ and $(\alpha)$, $(\beta)$, $(\nu)$ excited states, as well as $(\gamma)$, $(\delta)$, and $(\mu)$ for the photoionization from $^2B_1$ (EG) and $^2A_2$ (TS), respectively. Since neutral's vibrational wave function is delocalized alonog the pseudorotation coordinate over $^2B_1$ and $^2A_2$ states,[12] both sets of the cation's excited states can be produced in one electron photoionization.

Thus, all lowest excited states discussed in this work can contribute to the photoelectron spectrum, and, since they are close in energy and strongly coupled, the calculation of the full photoelectron spectrum becomes a challenging problem.

The Franck-Condon factors, however, are very different for many of the states. For example, the lowest excited states, $(\alpha)\,^1A_2$ and $(\alpha)\,^3A_2$, are almost dissociative along $C_{2v}$ distortion (see Table II) and collapse to linear equilibrium structures. Because of this geometry difference, the Franck-Condon factors for these $\alpha$ states and neutral $N_3$ are small, and they should produce only a background signal in the photoelectron spectrum. All other excited states are at least 3.8 eV higher than the cation ground state. Thus, the lower energy part ($E_{ex}<14$ eV) of the photoelectron spectrum can be well described as a transition from the $^2B_1/^2A_2$ pair of states of the neutral to the ground $X\,^1A_1$ state of the cation. Such calculation should include the geometric phase effect in neutral $N_3$ and will be presented elsewere.[32]

## VII. CONCLUSIONS

We described 12 lowest excited states of cyclic $N_3^+$. Eight lowest states (four singlets and four triplets) derived from single electronic excitations from doubly degenerate HOMO to doubly degenerate LUMO are close in energy at the ground state equilibrium geometry ($D_{3h}$) and exhibit a complicated Jahn-Teller behavior. Only two out of four states in each multiplicity are exactly degenerate and form an intersection seam along the symmetric stretch normal mode. However, this intersection is glancing rather than conical, because it is affected by interactions with two other nondegenerate states. Thus, adiabatic PESs do not have singularities at the intersections point, unless accidental triple degeneracy occurs. Therefore, these glancing intersections do not cause a geometric phase effect, which occurs in cyclic $N_3$ ground state or any other system with CI.

Stationary points of the excited states PES were also characterized. Cyclic $N_3$ ionization potential was estimated to be 10.595 eV, in a good agreement with recent experiments. The photoelectron spectrum of cyclic $N_3$ in the energy range $E_{ex}<14$ eV is predicted to be dominated by the transitions between the lowest electronic states of neutral $N_3$ and the ground state of the cation.

## ACKNOWLEDGMENTS

We are very grateful to Dr. Vladimir I. Pupyshev (Moscow State) for critical and insightful comments. We would also like to thank Alec Wodtke (UCSB) for helpful discussions and providing the experimental data. University of Southern California Center for High Performance Computing and Communications for making their computational resources available. A.I.K. acknowledges the support from the Department of Energy (DE-FG02-05ER15685).

[1] H. A. Jahn and E. Teller, Proc. R. Soc. London, Ser. A **161**, 220 (1937).
[2] I. B. Bersuker, Chem. Rev. (Washington, D.C.) **101**, 1067 (2001).
[3] V. I. Pupyshev, Int. J. Quantum Chem. **104**, 157 (2005).
[4] D. R. Yarkony, Rev. Mod. Phys. **68**, 985 (1996).
[5] *Conical Intersections. Electronic Structure, Dynamics and Spectroscopy*, edited by W. D. Domcke, D. R. Yarkony, and H. Köppel (World Scientific, Singapore, 2004).
[6] H. C. Longuet-Higgins, Proc. R. Soc. London, Ser. A **344**, 147 (1975).
[7] C. A. Mead and D. G. Truhlar, J. Chem. Phys. **70**, 2284 (1979).
[8] M. V. Berry, Proc. R. Soc. London, Ser. A **392**, 45 (1984).
[9] C. A. Mead, Rev. Mod. Phys. **64**, 51 (1992).
[10] W. H. Gerber and E. Schumacher, J. Chem. Phys. **69**, 1692 (1978).
[11] D. Babikov, B. K. Kendrick, P. Zhang, and K. Morokuma, J. Chem. Phys. **122**, 044315 (2005).
[12] D. Babikov, P. Zhang, and K. Morokuma, J. Chem. Phys. **121**, 6743 (2004).
[13] J. Wasilewski, J. Chem. Phys. **105**, 10969 (1996).
[14] M. Bittererová, H. Östmark, and T. Brinck, J. Chem. Phys. **116**, 9740 (2002).
[15] P. Zhang, K. Morokuma, and A. M. Wodtke, J. Chem. Phys. **122**, 014106 (2005).
[16] N. Hansen and A. M. Wodtke, J. Phys. Chem. A **107**, 10608 (2003).
[17] N. Hansen, A. M. Wodtke, S. J. Goncher, J. C. Robinson, N. E. Sveum, and D. M. Neumark, J. Chem. Phys. **123**, 104305 (2005).
[18] P. C. Samartzis, J. J. M. Lin, T. T. Ching, C. Chaudhuri, Y. T. Lee, S. H. Lee, and A. M. Wodtke, J. Chem. Phys. **123**, 051101 (2005).
[19] R. Tarroni and P. Tosi, Chem. Phys. Lett. **389**, 274 (2004).
[20] M. Goeppert-Mayer and A. L. Sclar, J. Chem. Phys. **6**, 645 (1938).
[21] J. M. O. Matos, B. O. Roos, and P.-A. Malmqvist, J. Chem. Phys. **86**, 1458 (1987).
[22] T. Hashimoto, H. Nakano, and K. Hirao, J. Mol. Struct.: THEOCHEM **451**, 25 (1998).
[23] M. H. Perrin and M. Gouterman, J. Chem. Phys. **46**, 1019 (1966).
[24] R. Meiswinkel and H. Köppel, Chem. Phys. **144**, 117 (1990).
[25] D. R. Yarkony, J. Chem. Phys. **111**, 4906 (1999).
[26] J. W. Zwanziger and E. R. Grant, J. Chem. Phys. **87**, 2954 (1987).
[27] T. J. Lee, D. J. Fox, H. F. Schaefer III, and R. M. Pitzer, J. Chem. Phys. **81**, 356 (1984).
[28] H. Koch, H. J. Aa. Jensen, P. Jørgensen, and T. Helgaker, J. Chem. Phys. **93**, 3345 (1990).
[29] J. F. Stanton and R. J. Bartlett, J. Chem. Phys. **98**, 7029 (1993).
[30] T. H. Dunning, J. Chem. Phys. **90**, 1007 (1989).
[31] R. Krishnan, J. S. Binkley, R. Seeger, and J. A. Pople, J. Chem. Phys. **72**, 650 (1980).
[32] D. M. Babikov, V. Mozhayskiy, and A. Krylov J. Chem. Phys.(submitted).
[33] P. Piecuch, S. A. Kucharski, and R. J. Bartlett, J. Chem. Phys. **110**, 6103 (1999).
[34] D. Feller, J. Chem. Phys. **96**, 6104 (1992).
[35] K. A. Peterson and T. H. Dunning, Jr., J. Chem. Phys. **102**, 2032 (1995).
[36] A. I. Krylov, Chem. Phys. Lett. **338**, 375 (2001).
[37] A. I. Krylov and C. D. Sherrill, J. Chem. Phys. **116**, 3194 (2002).
[38] J. Kong, C. A. White, A. I. Krylov *et al.*, J. Comput. Chem. **21**, 1532 (2000).
[39] J. F. Stanton, J. Gauss, J. D. Watts, W. J. Lauderdale, and R. J. Bartlett, ACES II, 1993. The package also contains modified versions of the MOLECULE Gaussian integral program of J. Almlöf and P. R. Taylor, the ABACUS integral derivative program written by T. U. Helgaker, H. J. Aa. Jensen, P. Jørgensen, and P. R. Taylor, and the PROPS property evaluation integral code of P. R. Taylor.
[40] Polar radius and angle are hyperspherical coordinates $\theta$ and $\phi$, which are similar to the bending and asymmetric stretch normal mode, respectively. For the precise definition stereographic coordinates, see Ref. 12 and references therein.
[41] H. Köppel, W. Domcke, and L. S. Cederbaum, *The Multi-mode Vibronic-Coupling Approach* (World Scientific, Singapore, 2004), Chap. 7, pp. 323–367.
[42] Wolfram Research, MATHEMATICA, http://www.wolfram.com/

[43] T. Carrington, Acc. Chem. Res. **7**, 20 (1974).
[44] T. Carrington, Faraday Discuss. Chem. Soc. **53**, 27 (1972).
[45] H. Köppel, *Jahn-Teller and Pseudo-Jahn-Teller Intersections: Spectroscopy and Vibronic Dynamics* (World Scientific, Singapore, 2004), Chap. 10, pp. 429–472.
[46] V. I. Pupyshev (private communication).
[47] S. Matsika and D. R. Yarkony, J. Chem. Phys. **117**, 5607 (2002).
[48] S. Matsika and D. R. Yarkony, J. Am. Chem. Soc. **125**, 10672 (2003).
[49] G. Halász, Á. Vibk, A. M. Mebel, and M. Baer, J. Chem. Phys. **118**, 3052 (2003).
[50] J. M. Dyke, N. B. H. Jonathan, A. E. Lewis, and A. Morris, Mol. Phys. **47**, 1231 (1982).